Novel Converter Concept for Bearingless Slice Motor Systems

Martin T. Bartholet, Thomas Nussbaumer, Peter Dirnberger*, Johann W. Kolar

Power Electronic Systems Laboratory
Swiss Federal Institute of Technology Zurich
8092 Zurich, SWITZERLAND
bartholet@eek.ee.ethz.ch

* LCM – Linz Competence Center of Mechatronics
4040 Linz, AUSTRIA

***Abstract*—The general trend towards smaller and more economical designs has also reached bearingless slice motor (BSM) systems. Up to now, full-bridge converters have been used in order to independently control the phases of the active magnetic bearing and the drive system. In this paper, a simplified topology based on three half-bridges is proposed to replace two conventional full-bridges. With this, the number of required power semiconductors is reduced by 25%. The three half-bridges can be advantageously realized by one integrated IGBT module, thus achieving a reduction of the total converter volume by 43% as compared to a discrete full-bridge solution. The principle of operation is explained and analytical expressions for the calculation of the current stresses on the power components and dc-link capacitors are provided as a basis for a design of the system. Finally, the performance of the system is shown for a 600W prototype of the topology.**

I. INTRODUCTION

Bearingless pump systems have been applied in different industries, such as the semiconductor and chemical processing industries, and for medical applications [1], [2]. In these applications the pumps must meet high requirements for purity and reliability (especially when the quality of these processes depends highly on the purity of the chemicals) and they have to resist very aggressive chemicals, such as acids, organic solvents and bases [3].

Meanwhile these types of bearingless pump systems (**Fig. 1**) are attracting more interest for applications in other industries such as electroplating and the food industry. However, in order to make the bearingless technology applicable for these new markets, the pump system must become economically more attractive. One major area to reduce the cost is the power electronics part of a bearingless slice motor (BSM) system. Therefore, new converter concepts have to be looked at that feature higher power density, higher efficiency and lower number of power switches.

In this paper first a novel interleaved half-bridge converter topology with a common bridge leg for the drive and bearing system of a BSM is presented and compared to a state-of-the-art full-bridge converter. After a short explanation of the principle of the BSM in **section II,** the novel topology is derived from the state-of-the-art full-bridge solution in **section III**. In **section IV** the operation principle of the novel converter is depicted and in **section V** the current stresses on the active and passive components of the system are calculated analytically. Finally, in **section VI,** a loss contribution is calculated and measurements on a 600W prototype of the converter driving a bearingless centrifugal pump are given in order to show the performance of the proposed system.

II. BEARINGLESS PUMP SYSTEM

The expression “bearingless motor” has been introduced in [4] for a rotating device without mechanical bearings. In order to stabilize the rotor contactless magnetic bearings are utilized. The bearingless slice motor (BSM) (cf. Fig. 1) is an advantageous realization of this concept in terms of higher compactness as has been shown in [5]. The BSM is analysed in detail in [5]-[7], therefore only a short description is given here.

Basically, the rotor has six spatial degrees of freedom that have to be stabilized magnetically through the housing wall. Three of them are stabilized passively, i.e. the axial displacement (in z-direction) and the angular displacement (tilting in x- and y-direction). The three remaining degrees of freedom are controlled actively, i.e. the radial displacement (in x- and y-direction) and the rotation of the rotor. Therefore, the active motor part generates the driving torque as well as the radial magnetic bearing forces, where active stabilization is facilitated with rotors that have a small height to diameter ratio.

A schematic of a typical bearingless motor which possesses two bearing phases B_1 and B_2 and two drive phases D_1 and D_2 is depicted in Fig. 1. In a conventional set-up each of these phases is controlled by a full-bridge converter, therefore resulting in four full-bridges employing four transistors and diodes each.

This motor configuration has a variety of advantages such as no rotating seals, no wear and no lubricants. A more detailed description of the advantages can be found in [5].

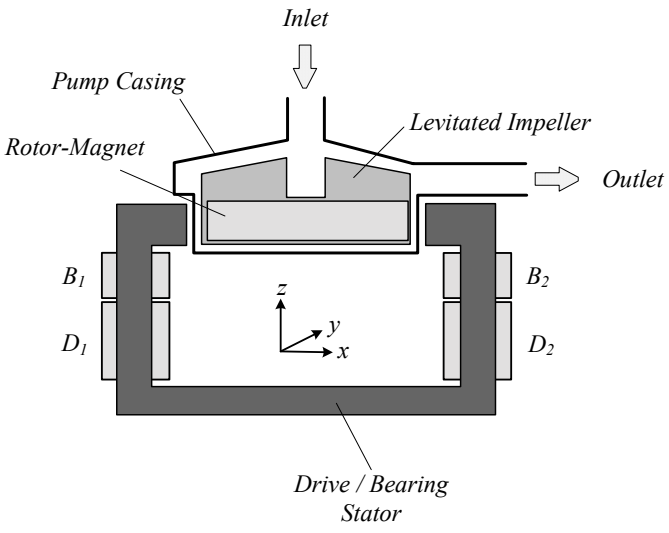

Fig. 1: Schematic of the basic principle of the bearingless centrifugal pump.

An overview of different motor concepts and their suitability for various applications is given in [6]. The control of the current, speed, and position is realized with a Digital Signal Processor. The control scheme of the bearingless slice motor is based on vector control and its principle is presented in [7].

Under load, and with no unbalance in the rotor, the currents in the bearing and drive windings are of sinusoidal shape. Under these conditions, a constant force, which results from the hydro dynamical pressure difference that is built up in the pump, is exerted on the impeller. This force, in turn, results in a radial displacement of the impeller which must be compensated by magnetic forces of the bearing. The bearing forces needed for the compensation require a bearing current, which is approximately sinusoidal. The two drive phases show a mechanical displacement of 90° and thus the currents in these coils have a phase shift of 90°. This fact will be important later when the drive and bearing currents are superposed.

III. CONVERTER CONCEPTS

A. Full-Bridge (FB) Topology

As stated above, in today's bearingless motor systems each phase of the bearing and drive system is driven by a full-bridge single-phase voltage source inverter from a DC voltage source supply. **Fig. 2**(a) shows one of the two bearing and drive full-bridges that are required for the control of the BSM. This set-up allows an independent adjustment of the currents in the bearing coils B_i and drive coils D_i and hence is the state-of-the-art topology for the control of a BSM. However, in terms of the number and utilization of the semiconductor switches it is inefficient, wherefore more compact solutions shall be investigated.

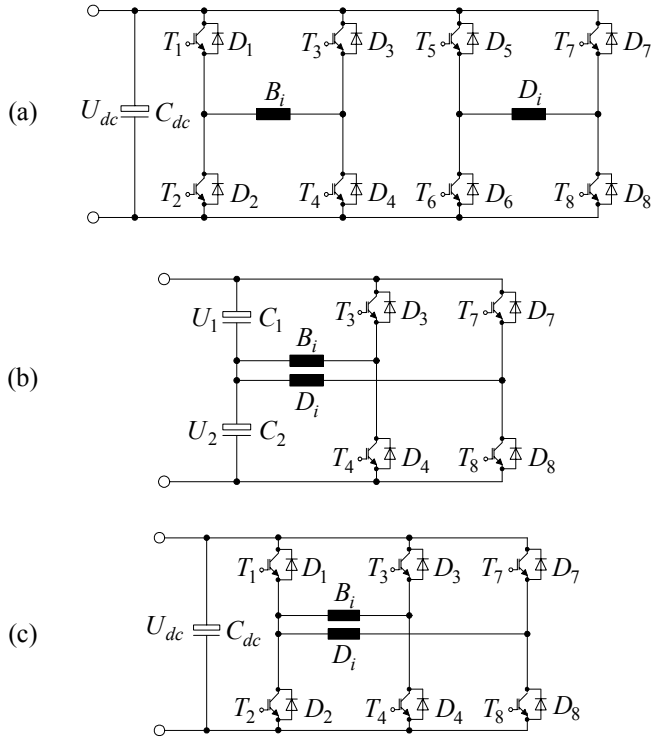

Fig. 2: Possible power electronic interfaces (a) State-of-the-art full-bridge topology for BSM for each drive (D_i) and bearing (B_i) winding, (b) split-capacitor topology and (c) interleaved half-bridge topology

B. Split-Capacitor (SC) Topology

The number of power semiconductors can be reduced if the two diode/IGBT combinations of the left bridge leg (T_1 /D_1, T_2 /D_2, T_5 /D_5, and T_6 /D_6) of the full-bridge topology are replaced by two capacitors, which are connected in series across the dc input and both drive and bearing coils are connected together with the junction of the two capacitors (cf. Fig. 2(b)). This junction is at a mid-potential, with a voltage $U_{dc}/2$ across each capacitor. Sufficiently large capacitors should be used in order to keep the potential at the junction of the two capacitors essentially constant with respect to the negative dc bus.

With this configuration the current direction in the drive and bearing windings can be controlled by only two switches per phase. In this way, the total number of switches, compared to the full-bridge topology, can be reduced from sixteen to eight.

However, this approach results in a higher control effort since the voltage of each capacitor must be accounted for additionally. In the case of a short circuit or unbalanced load, the voltage U_1 and U_2 can be significantly different from half the dc-link voltage. These unbalanced voltages across the two capacitors are unwanted and must be avoided, i.e. equalized. One approach to achieve equalized voltages is to control the current flowing in and out of the capacitors in addition to the control of the winding current. The d-component of the current in the drive windings can be used to control the capacitor voltages by varying the total current flowing through the capacitors. Since the q-component is needed to generate the torque of the motor which must be applied constantly, it cannot be varied in a certain operating point.

The problem of unbalanced voltages across series connected capacitors, which also occurs in switch-mode power supplies and welding converters, where two or more electrolytic capacitors are connected in series to form the dc-link, is further discussed in [8]. There, different concepts of active and passive balancing of the voltages across series connected capacitors are analysed.

In addition to the effort for stabilizing the capacitor middle-point a further system drawback is the limited control modulation. The maximum voltage applicable to the motor coils in this configuration is half the dc-link voltage. This limits the dynamic performance of the converter in transient conditions. Furthermore, for protection against earth fault conditions an additional switch has to be implemented that ensures a separation of the drive or bearing coil that causes the earth fault, from the capacitors. Therefore, this circuitry translates to additional effort. Summing up, this concept is not of interest for industrial applications.

C. Interleaved Half-Bridge (HB) Topology

The before-mentioned drawbacks of the split capacitor converter can be overcome by replacing the capacitors by an additional half-bridge [cf. Fig. 2(c)]. This topology in its basic form is already known from switched reluctance machines (SRM) [9], where one bridge leg is common for N phases of the SRM, resulting in N+1 inverter legs. However, this idea has not been employed until now in bearingless slice motor applications, where the common bridge leg (formed by T_1/D_1 and T_2/D_2) constitutes the connection point for a bearing and a drive winding.

If a fixed duty cycle of 50% is used for the common bridge leg, the connection point of the bearing and drive winding lies at the average potential of $U_{dc}/2$. This results in the same modulation range as for the split-capacitor topology. How-

ever, if higher torque is needed for the drive system, the duty cycle of the main bridge leg with the power-switches T_1 and T_2 can be varied so that a higher applicable voltage for the drive windings is obtained. With an adequate control algorithm it can be ensured, that the high dynamical requirements of the bearing system are still met.

The proposed circuit allows a realization of the controller with only six power half-bridges, resulting in a total of twelve switches, by offering the same control flexibility as the full-bridge converter. As a major advantage of this topology three phase intelligent power modules can be utilized for the realization of the three half-bridges as depicted in Fig. 2(c). These modules feature a three-phase inverter power stage with gate drivers and auxiliary circuitry in a compact, high performance, isolated package and are available off-the-shelf. Designing a converter in this way leads to more flexibility in the placement of the semiconductors. Furthermore, low inductive paths inside the modules provoke small overvoltages during switch-off transients. A drawback of the realization with modules is that they are usually not equipped with the cutting edge semiconductor technology.

D. Comparison

Several system advantages of the proposed interleaved half-bridge topology have already been mentioned. Finally, the data of the overall volumes and of the number of required switches is compiled in **Fig. 3** for the three topologies described before [cf. Fig. 2(a), (b) and (c)]. For this comparison an integrated half-bridge module [10] with a current rating of 20A is used for the interleaved half-bridge topology. For the realization of the full-bridge and the split capacitor topology discrete IGBTs [11] have been assumed. One can see, that the total amount of semiconductors needed is lowered by 25% for the half-bridge topology if realised with integrated modules. Due to the integration of the gate driver circuits and the protection circuitry in the modules the volume is even decreased by 43%.

Taking all this into account, the interleaved half-bridge topology is considered as the superior solution and will be investigated in the following sections.

IV. Principle of Operation

The modulation index M_i of a drive or bearing winding is defined by

$$M_i = \frac{\hat{U}_i}{U_{dc}}, \tag{1}$$

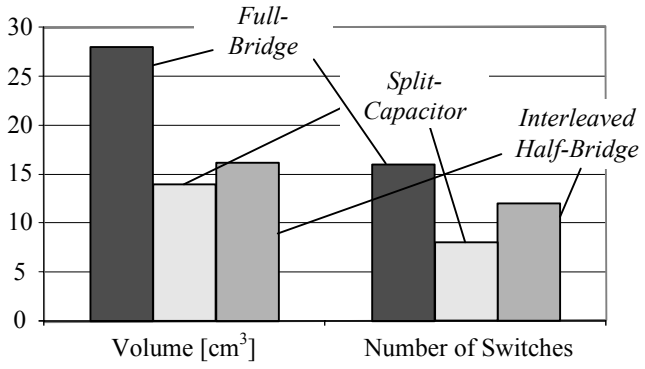

Fig. 3: Comparison of semiconductor volume [cm^3] and total number of switches for the different topologies: full-bridge topology (discrete), split-capacitor topology (discrete), and half-bridge topology (integrated modules).

where U_{dc} stands for the dc-link voltage and the voltage $\hat{U}_i$ defines the peak value of the clamp voltage u_i which is given by

$$u_i(t) = L_i \cdot \frac{di_i(t)}{dt} + R_i \cdot i_i(t) + u_{ind,i}(t) \tag{2}$$

according to **Fig. 4**. There, L_i denotes the inductance of one bearing or drive coil, R_i the ohmic resistance of that coil and $u_{ind,i}$ the induced voltage in the bearing or drive winding. The induced voltage in the bearing winding cannot be neglected generally, since the radial movement of the magnet can induce a considerable voltage in that bearing depending on the actual circuit configuration and thus appears in the calculation of the modulation index as well.

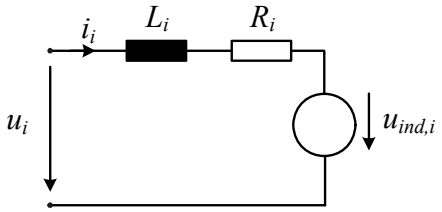

Fig. 4: Equivalent circuit of one bearing or drive coil.

The interleaved half-bridge controller is operated with unipolar control as described in [12]. The switches in the two legs are controlled separately by comparing the triangular signal u_{tri} with control signals δ_{Ti}. E.g., for the control of the current in the bearing coil B_1 [cf. Fig. 2(c)] the comparison of the relative duty cycles δ_{T1} of the transistors T_1 and T_3 with the triangular waveform results in the modulation depth M_{Bi} given by

$$\begin{aligned} M_{Bi} &= \delta_{T1} - \delta_{T3} \quad for \quad -\pi/2 < \varphi < \pi/2 \\ M_{Bi} &= \delta_{T3} - \delta_{T1} \quad for \quad \pi/2 < \varphi < 3\pi/2 \end{aligned}, \tag{3}$$

where $\varphi = \omega t$ is the phase angle of the current $i_{i(t)}$. This easiest realisation of that modulation method results if the duty cycles δ_{Ti} are kept constant during a half cycle of the current sine wave. As depicted in **Fig. 5** this results in a triangular current shape. A larger current ripple and higher rms components occur for this modulation method compared to a pure sinusoidal current which can be obtained by sinusoidal control signals δ_{Ti}. However, for the sake of simplicity in this paper the modulation with constant duty cycles is employed.

As stated in section III.C, as a nominal operation point a duty cycle of $\delta_{Ti} = 0.5$ can be adjusted. If a higher torque and thus a higher current in the drive system is needed than is available with half the dc-link voltage [cf. Fig. 2(c)], an additional control loop must be implemented in order to vary the duty cycle of the switches in the common bridge leg in such a way that the potential of the connection point of these switches and the drive and bearing windings is virtually shifted up or down. This must be done without limiting the control stability of the bearing system.

V. Stresses on the Power Components

In the following, the performance of the proposed system is evaluated by calculation of the current stresses on the active and passive components and later on the power losses.

The stresses on the power components are calculated analytically with dependency on the operating points of the pump. The calculations are based on the following assumptions:

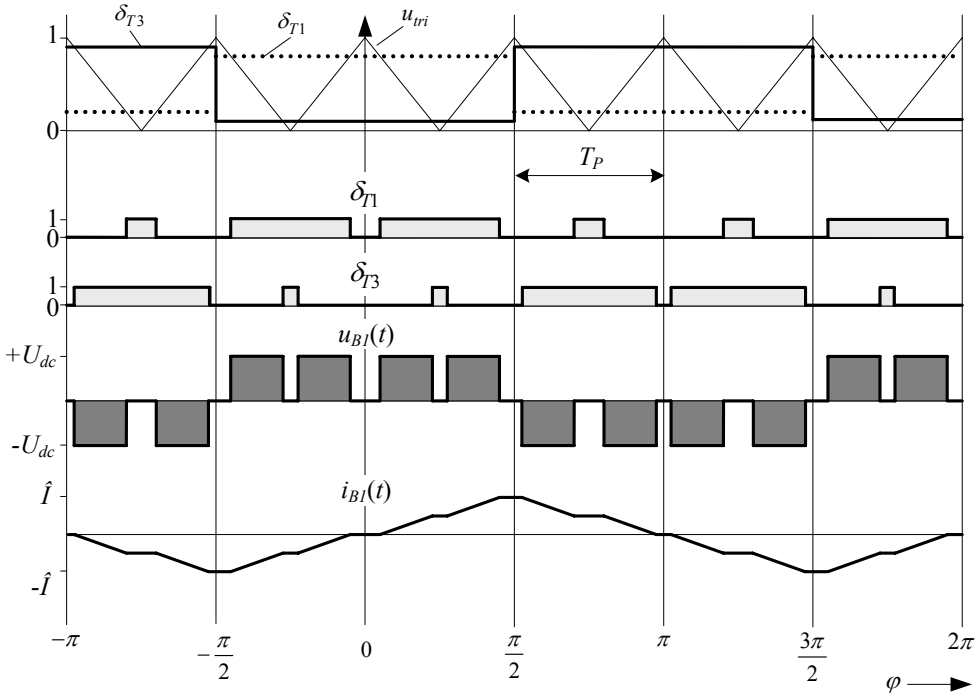

Fig. 5: Switching pattern of the bearing bridge-leg of the interleaved half-bridge topology. For terms of easier explanation a very low switching frequency $f_S = 1/T_P = (2\omega)/\pi$ has been chosen, i.e. only one switching pattern occurs during a quarter current period.

1) Pure sinusoidal current in the drive and bearing system under load as stated in section III.
2) Constant input current.
3) Stresses on the dc-link capacitors caused by the input side (diode bridge, PFC) of the converter are neglected.

In order to obtain the stresses on the active and passive components it is necessary to calculate the average and rms values of the device currents. For an exact calculation of the global average current values the contributions of each pulse interval have to be determined and summed up over a whole mains period.

As stated in [13], the summation can be replaced by an integration of the local averaged values over the mains period under the assumption, that the switching frequency is sufficiently higher than the fundamental frequency of the switched current.

$$I_{i,avg} = \frac{1}{2\pi}\int_0^{2\pi}\left(\frac{1}{T_p}\int_0^{T_p} i_i(\varphi,t_\mu)dt_\mu\right)d\varphi\,, \tag{4}$$

where

$$\varphi = \omega\, t \tag{5}$$

defines the actual position of a pulse interval within a mains period. Analogously, the square of the global rms value can be found by integration of the square local rms value

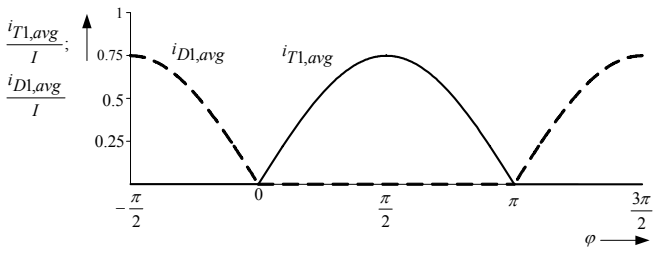

Fig. 6: Time behavior of the local average values of the currents of the power transistor T_1 and the freewheeling diode D_1 for a duty cycle $\delta_{T1} = 0.75$.

$$I^2_{i,rms} = \frac{1}{2\pi}\int_0^{2\pi}\left(\frac{1}{T_P}\int_0^{T_P} i_i^2(\varphi,t_\mu)dt_\mu\right)d\varphi\,. \tag{6}$$

With this, the component stresses can be evaluated analytically. The time behaviour of the local average values of the transistor T_1 along with the freewheeling diode D_1 of the interleaved half-bridge topology (cf. Fig. 2(c)) is shown in **Fig. 6**. The resulting average and rms values for all devices are compiled in **Fig. 7**.

For the interleaved half-bridge topology the current in the transistors T_1 and T_2 is the sum of the bearing current i_{Bi} and drive current i_{Di}. Thus, the stresses on these components are higher than for the other switches and diodes in this topology.

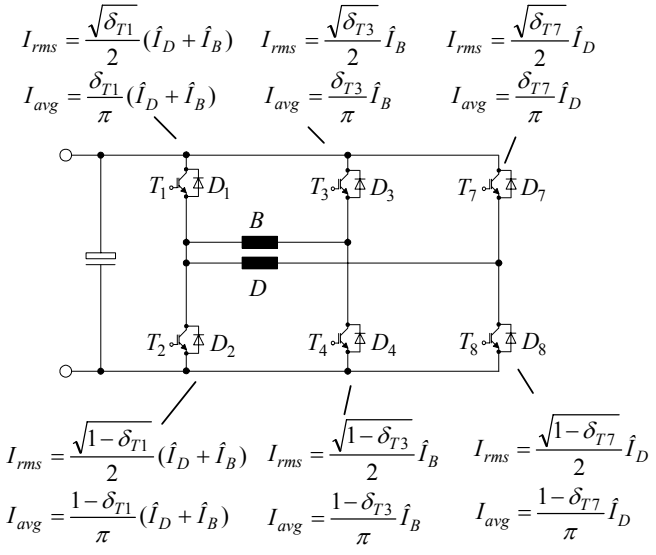

Fig. 7: Analytical approximations of average and rms values of the component currents for the interleaved half-bridge topology in dependency of the current $\hat{I}$ in the bearing and drive coil. The rms and average values are the same for the transistors T_i and the diodes D_i of each combination T_i/D_i.

A. Semiconductor Stresses

Calculation of Switching Losses

As can be seen in Fig. 5, there are four switching instants during every pulse period, where switching losses occur, e.g. for $0 < \varphi < \pi/2$:

- Turn-on of switch T_1 after the freewheeling state (between D_2 and T_4) and commutation of the current from D_2 to T_1. Turn on losses in the switch and reverse recovery losses in the freewheeling diode occur.
- Turn-off of switch T_4 and commutation of the current to the freewheeling diode D_3. Turn-off losses in the switch occur.
- Turn-on of switch T_4 and commutation of the current from D_3 to T_4. Turn on losses in the switch and reverse recovery losses in the freewheeling diode occur.
- Turn-off of switch T_1 and commutation of the current to the freewheeling diode D_2. Turn-off losses in the switch occur.

Due to the symmetry of the used switching pattern and the utilization of similar components for all bridge legs it is sufficient to integrate the loss energy of each loss term over a $\pi/2$-wide interval

$$P_{Sw} = f_s \cdot \frac{2}{\pi} \int_0^{\pi/2} w(u,i) d\varphi \,. \tag{7}$$

Assuming a linear dependency of the loss energy on current and voltage

$$w(u,i) = k \cdot u \cdot i \,. \tag{8}$$

a switching losses calculation based on manufacturer's data can be performed, where component specific factors k_{on}, k_{off} and k_{rev} for the turn-on, the turn-off and the reverse recovery losses, respectively, can be utilized.

With this, the resulting switching losses due to the bearing current are the sum of the turn on ($P_{Sw,on}$) and turn off ($P_{Sw,off}$) losses occurring in two of the four IGBTs involved in the switching of the bearing current

$$\begin{aligned} P_{Sw,IGBT,B} &= 2 \cdot P_{Sw,on,B} + 2 \cdot P_{Sw,off,B} = \\ &= 2 \cdot f_s \cdot \frac{2}{\pi} \int_0^{\pi/2} (k_{on} + k_{off}) \cdot (\hat{I}_B \cdot \sin\varphi)\, d\varphi = \\ &= \frac{4 \cdot f_s}{\pi} \cdot (k_{on} + k_{off}) \cdot \hat{I}_B . \end{aligned} \tag{9}$$

For the switching losses of the freewheeling diode only the reverse recovery losses are considered

$$\begin{aligned} P_{Sw,DF,B} &= f_s \cdot \frac{2}{\pi} \int_0^{\pi/2} 2 \cdot k_{rev} \cdot (\hat{I}_B \cdot \sin\varphi)\, d\varphi = \\ &= \frac{4 \cdot f_s}{\pi} \cdot k_{rev} \cdot \hat{I}_B , \end{aligned} \tag{10}$$

since the forward recovery losses in the diodes can be neglected.

The switching losses of the semiconductors in the bearing half-bridge are therefore given by

$$P_{Sw,T3} = P_{Sw,T4} = \frac{P_{Sw,IGBT,B}}{4} , \tag{11}$$

and

$$P_{Sw,D3} = P_{Sw,D4} = \frac{P_{Sw,DF,B}}{4} . \tag{12}$$

The switching losses $P_{SW,IGBT,D}$ and $P_{SW,DF,D}$ in the drive path can be calculated analogously.

Since a linear dependency of the losses on the switched current has been assumed (8), the switching losses of the semiconductors in the common bridge leg can be superposed by the losses in the bearing and the drive bridge leg:

$$P_{Sw,T1} = P_{Sw,T2} = \frac{P_{Sw,IGBT,B} + P_{Sw,IGBT,D}}{4} , \tag{13}$$

$$P_{Sw,D1} = P_{Sw,D2} = \frac{P_{Sw,DF,B} + P_{Sw,DF,D}}{4} . \tag{14}$$

Calculation of Conduction Losses

The forward characteristics of the semiconductors can be approximated by a forward voltage drop and a forward resistance. The parameters $U_{CE,0}$ and r_{CE} for the IGBT, and $U_{F,0}$, r_D for the diode, respectively, are given in the datasheets [10],[11]. With this, the conduction losses of any semiconductor i can be derived by

$$P_{Fw,Ti} = U_{CE,0} \cdot I_{Ti,avg} + r_{CE,on} \cdot I_{Ti,rms}^2 , \tag{15}$$

$$P_{Fw,Di} = U_{F,0} \cdot I_{Di,avg} + r_D \cdot I_{Di,rms}^2 . \tag{16}$$

B. Input Capacitor

In the following the current stress of the input capacitor of the interleaved half-bridge topology is calculated. Since the current in the common bridge leg is a superposition of the currents in the drive and bearing windings, the configuration of two full-bridges [Fig. 2(a)] is equivalent in terms of the capacitor current. Therefore, for reasons of better clearness the subsequent explanations are carried out for the full-bridge topologies which gives the same result as for the proposed topology.

During every $\pi/2$-period the current $i_{FB,i}(t)$ of the drive or bearing system that flows into the converter (cf. **Fig. 8**) during the active state is defined as

$$i_{FB,i}(t) = M_i \cdot \hat{I}_i \cdot \sin \omega t \,. \tag{17}$$

With this, the average and rms current flowing into the full-bridge over one period is calculated by

$$I_{avg,FB,i} = \hat{I}_i \frac{2M_i}{\pi} , \tag{18}$$

$$I_{rms,FB,i} = \hat{I}_i \sqrt{\frac{M_i}{2}} , \tag{19}$$

where M_i denotes the modulation index of the bearing or drive system and i stands for one of the two bearing/drive systems.

As an immanent property of the BSM technology the bearing currents are in phase with their respective drive currents as explained in section II and therefore the rms value of these two correlated and in-phase currents can be added directly to build the total current of that drive and bearing combination as described in [14]. With this, the total rms-value of each drive and bearing coil can be derived by

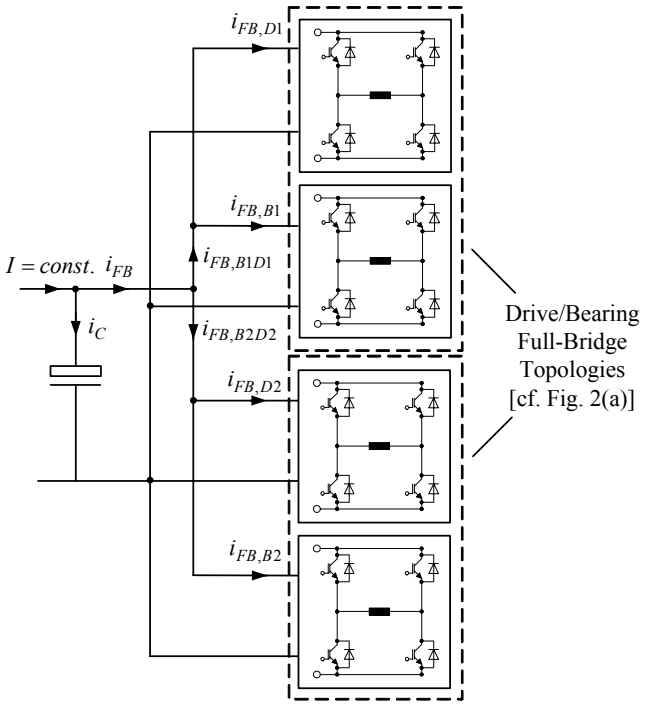

Fig. 8: Configuration of the bearing and drive system employing four full-bridge converters.

$$I_{FB,B1D1,rms} = I_{FB,B1,rms} + I_{FB,D1,rms} = \\ = I_{FB,B2D2,rms} = I_{FB,B2,rms} + I_{FB,D2,rms} \tag{20}$$

This produces the worst case capacitor rms current value as can be seen in **Fig. 9**(a).

Combining (19) and (20) leads to the following relationship between the total current of one bearing and drive system that is flowing into the two full-bridges of that system and thus must be supported by the dc-link capacitor.

$$I_{FB,B1D1,rms} = I_{FB,B2D2,rms} = \frac{1}{\sqrt{2}}(\hat{I}_B\sqrt{M_B} + \hat{I}_D\sqrt{M_D}) . \tag{21}$$

As stated before, the phase shift between the two drive currents is $\pi/2$. As further described in [14] the rms values of these currents cannot be added in the same way as it can be done for the correlated drive and bearing currents. Thus, the sum of (21) for the two systems is

$$I_{FB,rms} = \\ = \sqrt{\frac{1}{2\pi}\int_0^{2\pi}(I_{FB,B1D1,rms}\sin(\varphi) + I_{FB,B2D2,rms}\cos(\varphi))^2 d\varphi} = \\ = \frac{1}{\sqrt{2}}(\hat{I}_B\sqrt{M_B} + \hat{I}_D\sqrt{M_D}). \tag{22}$$

Therefore, due to the $\pi/2$ phase shift of the two currents this results in the same current value as for one of the two systems. This current must be supported by the input capacitor of the converter.

The total average current $I_{FB,avg}$, which is the sum of the four average currents (cf. Fig. 8) flowing into the bridges, is

$$I_{FB,avg} = \frac{4}{\pi}(\hat{I}_B M_B + \hat{I}_D M_D) . \tag{23}$$

The instantaneous dc-link capacitor current is defined by the difference between the constant converter input current I and the total input current i_{FB} of all four full-bridges:

$$i_C(t) = I - i_{FB}(t) . \tag{24}$$

Assuming sinusoidally shaped bearing and drive currents (17), the rms-value of the input capacitor current for the full-bridge topology is given by

$$I_{C,rms}^2 = I_{rms,FB}^2 - I_{avg,FB}^2 , \tag{25}$$

and with Eq. (22) and (23)

$$I_{C,rms} = \\ \sqrt{(\frac{1}{\sqrt{2}}(\hat{I}_B\sqrt{M_B} + \hat{I}_D\sqrt{M_D}))^2 - (\frac{4}{\pi}(\hat{I}_B M_B + \hat{I}_D M_D))^2} . \tag{26}$$

Eq. (26) represents the desired functional dependency of the capacitor current stress on the pump operating parameters.

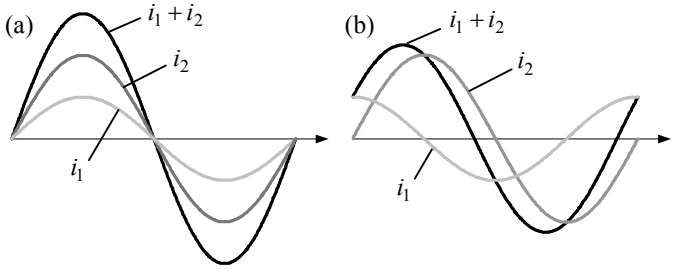

Fig. 9: Determination of the rms current for correlated (a) and $\pi/2$ phase-shifted currents (b).

VI. Performance Investigation

A. Power Loss Distribution

Based on the analytical equations of the loss terms the loss contributions of the switching components can be derived straight-forward. In **Fig. 10** the losses are shown for f_s = 20kHz switching frequency, an estimated junction temperature T_J = 150°C and a dc-link voltage of U_{dc} = 320V for different operation points of the pump under load. The flow through the pump is regulated to a constant flow of 15l/min. This results in an output pressure of 0.07bar for 2000 rpm, 0.45bar for 4000rpm and 1.25bar for a rotor speed of 6000rpm, which corresponds to electrical power values of 94W, 167W, and 300W, respectively.

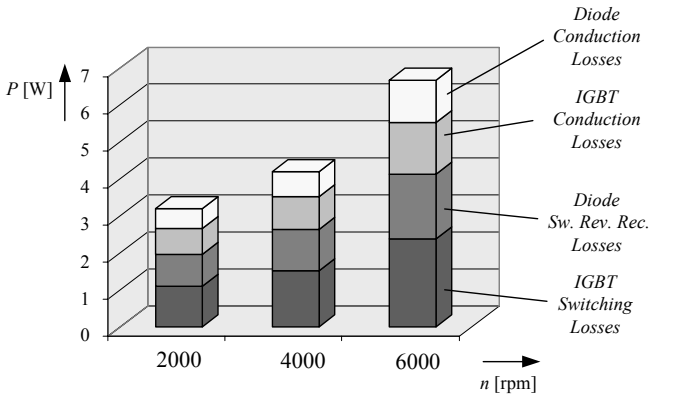

Fig. 10: Total losses of the switches and diodes of the interleaved half-bridge converter for constantly regulated flow of 15l/min, U_{dc} = 320V, f_S = 20kHz, T_J = 150°C. Due to the constant flow of the pump the rotation speeds of n = 2000rpm, 4000rpm, and 6000rpm correspond to different electrical power values of 94W, 167W, and 300W, respectively.

Fig. 10 shows that switching and conduction losses are well balanced over the investigated power range. Furthermore, the losses are distributed equally between the diodes and the IGBTs. However, it has to be stated that these calculations are

only approximations based on interpolated data extracted from the datasheets which can differ from real switching loss values depending on the utilized gate resistances and on the PCB layout. For an accurate calculation, they have to be identified by switching loss measurements on the prototype.

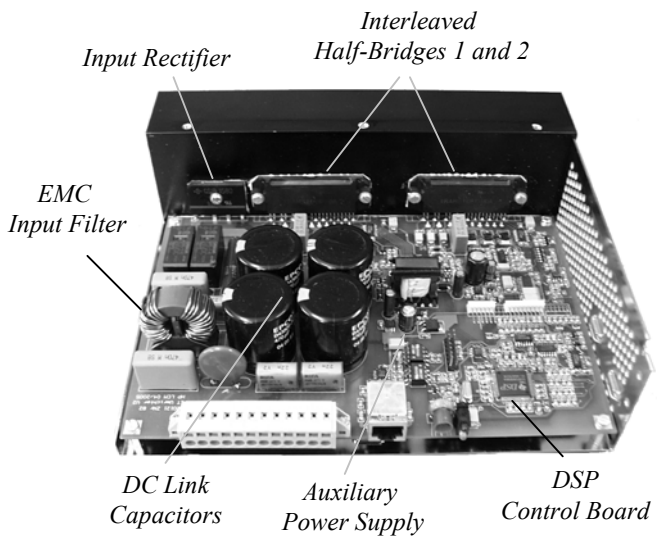

Fig. 11: Prototype of the 600W interleaved half-bridge converter.

B. Experimental Setup

In order to verify the concept of the interleaved half-bridge topology a 600W prototype with integrated half-bridge power modules [10], which is operated from a single phase mains voltage, has been built (cf. **Fig. 11**). This converter operates a bearingless pump, which has a rated electrical power of 600W and the number of turns of the drive and bearing coils are designed to suit a dc operating voltage of U_{dc} = 160V. The currents in the drive and bearing system for a rotor speed of 7000rpm are shown in **Fig. 12**.

VII. CONCLUSIONS

This paper presents a novel converter configuration for bearingless slice motor systems, which is formed by integration of two half-bridge legs to a common bridge leg for a drive and a bearing winding. This leads to a significant reduction of 25% for the amount of required semiconductors as compared to a state-of-the-art full-bridge realisation and the total volume of the switching components is reduced by 43%. Advantageously, intelligent three-phase modules comprising three full-bridges, gate drivers and protection circuitry can be utilized, enabling facile assembling and a highly compact design.

The given analytical expressions for the current stresses of the power semiconductors and dc-link capacitor allow a design of the system by the knowledge of the expected drive and bearing currents and the desired modulation range. A contribution of the semiconductor loss terms has shown that the switching and the conduction losses are well balanced throughout the operation range of interest. Through a realization of a 600W prototype of the system the principal system functionality has been proven.

In a next step, an optimum modulation method will be identified with the goal to achieve minimum losses in the inverter stages as well as optimum steady state and dynamical pump performance while ensuring the required modulation range for the bearing system. Furthermore, the performance of the modules will be investigated in detail, such as the analysis of the switching behavior and the development of a thermal model of the system.

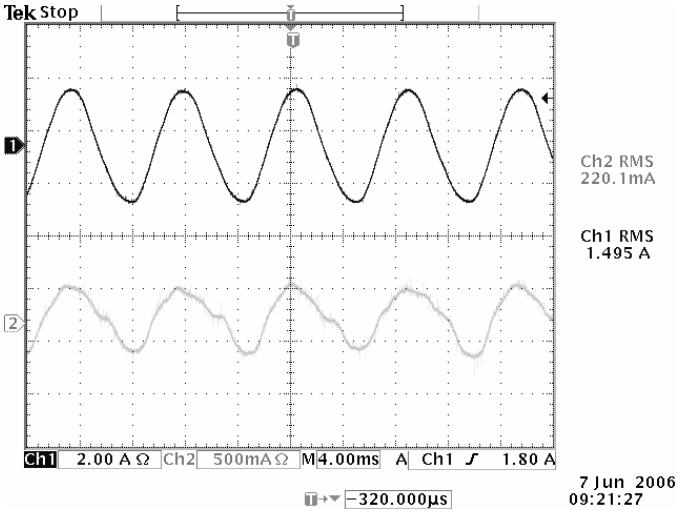

Fig. 12: Current waveforms measured at the 600W interleaved half-bridge converter (channel 1: drive current, 2A/div., channel 2: bearing current, 500mA/div., time scale: 4ms/div.).

REFERENCES

[1] N. Barletta, R. Schöb, "Design of a Bearingless Blood Pump", 3rd International Symposium on Magnetic Suspension Technology, Florida, December 13-15, 1995, pp.265-274.

[2] P.N. Bösch, N. Barletta, "High Power Bearingless Slice Motor (3-4kW) for Bearingless Canned Pumps", 9th International Symposium on Magnetic Bearings, Lexington, Kentucky, USA, August 3-6, 2004.

[3] M. Neff, N. Barletta, R. Schöb, "Magnetically levitated centrifugal pump for highly pure and aggressive chemicals", PCIM Conference 2000, Nuremberg/Germany, June 6-8, 2000.

[4] J. Bichsel, "Beiträge zum lagerlosen Elektromotor", Dissertation ETH Zürich, 1990.

[5] R. Schöb, N. Barletta, J. Hahn, "The Bearingless centrifugal pump – A perfect example of a mechatronics system", 1st IFAC-Conference on Mechatronic Systems, Darmstadt, Germany, 18-20 September 2000.

[6] S. Silber, W. Amrhein, P. Bösch, R. Schöb, N. Barletta, "Design Aspects of a Bearingless Slice Motor", Mechatronics, IEEE/ASME Transactions on, Volume 10, Issue 6, Dec. 2005 Page(s): 611 – 617.

[7] R Schöb, J. Bichsel, "Vector Control of the Bearingless Motor", 4th International Symposium on Magnetic Bearings, Zurich 1994.

[8] H. Ertl, T. Wiesinger, J.W. Kolar, F.C. Zach, "A Simple Active Method to Avoid the Balancing Losses of DC Link Capacitors", 24th International Conference on Power Electronics (PCIM), Nürnberg, Germany, May 20-22, 2003.

[9] Z. Grbo, S.Vukosavić, E. Levi, "A Novel Power Inverter for Switched Reluctance Motor Drives", Elec. Energ., vol. 18, no. 3, December 2005, pp. 453-465.

[10] International Rectifier: Integrated Hybrid IC IRAMX20UP60A. Datasheet (2005).

[11] International Rectifier: Ultrafast IGBT IRG4PC50KD. Datasheet (2004).

[12] N. Mohan, T.M. Undeland, W.P. Robbins, "Power Electronics: Converters, Applications and Design." 2nd Edition, 1995, New York: John Wiley&Sons.

[13] J.W. Kolar, H. Ertl, and F.C Zach, "A Comprehensive Design Approach for a Three-Phase High Frequency Single-Switch Discontinuous-Mode Boost Power Factor Corrector Based on Analytically Derived Normalized Converter Component Ratings", IEEE Trans. Ind. Appl., vol. 31, no.3, May/Jun, pp. 569-582, 1995.

[14] J.W. Kolar, S. Round, "Analytical Calculation of the RMS Current Stress on the DC Link Capacitor of Voltage PWM Converter Systems", in press. IEE Proc. Electric Power Applications.